COPPER EXTRACTION FROM HYDROTHERMAL POLYMETALLIC ORE SOURCES IN MEYMAND CAVE DWELLING VILLAGE, IRAN; AN ARCHAEOMETALLURGICAL APPROACH

EXTRACCIÓN DE COBRE DE YACIMIENTOS HIDROTERMALES POLIMETÁLICOS DE LA CAVERNA DE MAYMAND, IRÁN; UN ENFOQUE ARQUEO-METALÚRGICO

Mohammadamin Emami

Faculty of Conservation and Archaeology,
Art University of Isfahan, Iran 2. Departament of Building Material Chemistry,
University Siegen, Germany República Islámica de Iran

Mohammadamin, E. (2013). *Copper extraction from hydrothermal polymetallic ore sources in meymand cave dwelling village, Iran; and archaeometallurgical approach.* GEOLOGIA COLOMBIANA, Vol. 38. Bogotá, Colombia. pp. 159-172.

Manuscrito recibido: 13 de marzo de 2012; aceptado: 1 de junio de 2013

Abstract

The polymetallic ore intrusion of "Meymand" is situated between three important copper and iron orogeny zones called "Sarcheshmeh", "Meydook" and "Gol-e Gohar" in the Kerman province, central Iran. The occurrences of polymetallic sulphide intrusions (Cu, Cu+Fe+As, Cu+Au+Fe, Cu+Zn) with various metallic ore compositions are also one of the reasons why this region belongs to the most significant areas for the beginning of metallurgy on the Iranian plateau.

The main motivation for this research is the characterization of the smelting slags used for metallurgical purposes in Meymand, based on quantitative XRD methods, including the Rietveld phases refining method. Through polarization microscopy, the interpretation of the paragenesis of the phases in the solid is possible, as well as in the fluid state. Atomic force microscopy in non-contact mode was used in order to obtain some information on the topography and roughness of slag matrices during the smelting process, according to the recrystallization segregation.

With respect to the mineralogical phase, segregation silicates mainly consist of augite, fayalite, and clinoferrosilite. The main oxides are hematite and magnetite. Metallic phases are known as copper and iron (wüstite). According to the thermodynamic stability field of minerals in the pyroxen bearing slag, copper extraction was carried out at approximately 890°C.

Keywords: Archaeo-metallurgy, economic geology, copper, hydrothermal, QXRD, AFM, Iran.

Resumen

La intrusión de minerales polimetálico de cobre y hierro en "Meymand", se sitúa entre tres importante zonas orogénicas llamadas "Sarcheshmeh", "Meydook" y "Gol-e Gohar", en la provincia de Kerman, en el centro de Irán. Las ocurrencias de las intrusiones de sulfuro polimetálico (Cu, Cu + Fe + As, Cu + Au + Fe, Cu + Zn) con diversos minerales metálicos son también una de las razones por las que esta región pertenece a las áreas más significativas para el comienzo de la metalurgia en la meseta iraní.

La principal motivación de esta investigación es la caracterización de las escorias de fundición utilizadas para fines metalúrgicos en Meymand, basado en métodos de DRX cuantitativos, incluyendo el método de refinado de fases de Rietveld. Mediante microscopía de polarización, es posible la interpretación de la paragénesis de las fases en el sólido, así también en el estado fluido. Se utilizó la microscopia de rayos atómicos en modo sin contacto, para obtener información sobre la topografía y rugosidad de las matrices de escoria durante el proceso de fundición, según la recristalización de la segregación. Con respecto a la fase mineralógica, los silicatos de segregación presentes consisten principalmente en augita, fayalita y clino-ferrosilita. Los principales óxidos son la hematita y la magnetita. Las fases metálicas se conocen como cobre y hierro (wüstite). De acuerdo con el campo de estabilidad termodinámico de los minerales de piroxeno en la escoria, la extracción de cobre fue llevada a cabo a aproximadamente a 890 °C.

Palabras clave: Arqueo-metalurgia, geología económica, cobre, hidrotermal, QXRD, AFM, Irán

INTRODUCTION

This paper discusses a recently explored archaeo-metallurgical workshop in south-central Iran. This is a preliminary report on an ongoing project, and no archaeological studies have been carried out yet on the site. Archaeological studies are planned for the near future, but, in this paper, only the possible correlation of the mining area with the smelting residues has been researched.

The cave dwelling village of Meymand, is built in the magmatite formations in the central-southern part of Iran, which is covered by a thick layer of tuff (Fig.1). Its geographical coordination is 55° 23′ eastern longitude and 30° 14′ northern latitude (NGO of I.R.IRAN 2003). The closest city to Meymand is Shar-e Babak, which also belongs to the geologically famous formation in central Iran. This area covers the mountainous area of Nar-Kuh, Kuh-e Masahim and Pa-Qaleh, with altitudes of over 2200 m.

Meymand is a historical village that was quarried in mountain walls of a granodiorite-diorite formation (Ebrahimi Meymand, 2002). Archaeological investigations in this village indicate that the history of the settlement in this area might go back to the 1st millennium BC (Izadpanah, 2002). The "Lasoleyman" archaeometallurgical area is located at 4 km southeast of the Meymand village around the Khah-kuh Mountain, in the Lasoleyman valley region (Fig. 2). The mineralogical-chemical analysis was carried out on remains of metallurgical activities, such as slags and ores.

Characterization of slags as well as ores suggests the relationship between raw material usage and metallurgical remains for metal extracting in this region. On the other

Figure 1. View of Meymand cave dwelling village.

Figure 2. Geographical Location of Meymand and Lasoleiman archaeometallurgical site in Central Iran.

hand, petrographical investigation on the textural properties of the slag, as well as bulk chemical composition of these materials, gives us information about the accidental or experimental metallurgy in this region.

Due to the location of Meymand in central Iran, its closeness to the important economic ore deposits and also the existence of metallurgical evidences in this area, the scope of the study may be summarized as follows:

- An experimental interpretation of the extraction techniques based on slag petrography.
- A possible connection between technological features and the kind of raw material used for metallurgy in this area.
- Application of AFM for characterising the phase transition and evaluation.

GEOLOGICAL SETTING

The site is situated in the centre of the valley and has an extension of about 1000 m^2. Slag dump sites are concentrated in two separate areas that extend in a north-south orientation.

According to earlier studies in north-central Iran, Cu and Cu+As, extraction technology and alloying process developed through the exploitation of successive intrusions from gabbroic to syenitic and quartz saturated granitic rocks (Emami, 2006). Metallurgical traces consist of slag and broken ceramics. Additionally, some remains of beneficiated stone pieces, containing low amounts of ore, are found. Preliminary field investigations were able to find furnace remains.

Archaeo-metallurgical research on the regional sulphide ore resources in this site, allows the reconstruction of nomadic but cognizant metallurgy at this area. The area described in this paper forms part of a northwest-south-east positioned mountain chain consisting mainly of Tertiary lavas and tuffs (Fig.3).

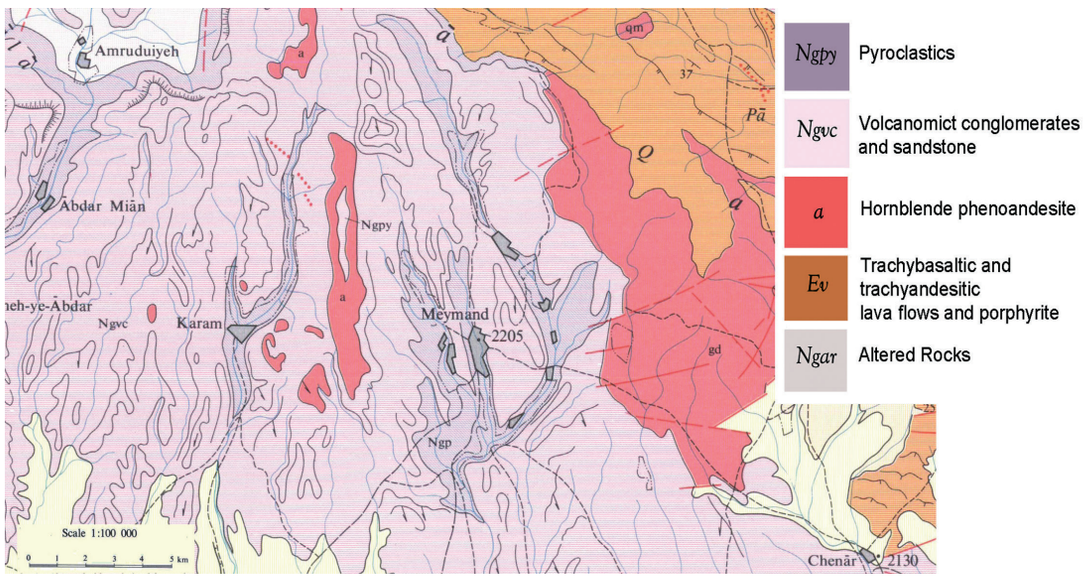

Figure 3. Geological formation of Meymand and Lasoleiman in Central Iran.

The most prominent stratigraphic feature in the investigated area is a transgressive limestone overlapping progressively the metamorphic rocks from west to east, color melange and the "Alimoradi Formation". This limestone-termed the "Saidabad Limestone Member"-overlays a sequence of coarse grained sandstone and conglomerate containing limestone.

This formation, collapsed in the south with the "Chahr Gonbad Formation", is very important because of its metallic ore bearing intrusions. The mineralization forms rich swelling and pinching veins, also in lenses and/or disseminations. The primary ore is chalcopyrite, chalcosite and pyrite, and a very minor amount of galena. The gangue minerals are calcite and quartz. The plagioclase and feldspar minerals are common minerals contained in the rock formation in the region.

In some cases there is albite, associated with biotite, due to the albitization process. This paragenesis developed mainly through formation under hydrothermal conditions (Ness, 2004). Secondary minerals are malachite, azurite, bornite, siderite, dolomite, rhodochrosite and very little gypsum. In the Meymand area, several forms of mineralization can be distinguished;

1. Mineralization associated with faults and fault intersections.
2. Veined mineralization in diorite-porphyrite, sedimentary and volcanic rocks.
3. Mineralized interface between diorite-porphyrite and sediments.
4. Veined mineralization partly concordant with stratification in sedimentary rocks.
5. Mineralization along plane of transgression between andesite and limestone.

The common economic ores are mainly chalcopyrite, pyrite, chalcocite, siderite and hematite. The main economic ore formations in this region are hydrothermal ore deposits, such as copper and iron. Copper layers are settled within huge sequences of iron (NGO of I.R.-IRAN, 2003). Hydrothermal copper and subordinate lead occurrences are scattered throughout the northern part of this area. The Lasoleiman occurrence is of the porphyry copper type, containing Cu-carbonate, chrysocolla and limonite in the zone of superficial alterations, together with primary pyrite and disseminated chalcopyrite. Vein type Cu, mineralisation occurs at Chah-Messi with pyrite, chalcopyrite and galena as well as in area of Chehel Dokhtatarn. In this sequence, quartz veins contain magnetite and malachite. On the south slope of this area there is a hydrothermally altered bearing Cu and Pb mineralization. This mineralization is, at least partly, related to Neogene volcanism.

SAMPLE DESCRIPTION AND METHODOLOGY

Lasoleiman is located in the south part of the Zagros polymetallic orogeny and south east of Meymand village. Archaeo-metallurgical sampling has been carried out on the preserved metallurgical workshop residues, i.e. on the slag found on the surface. In the Lasoleiman area, two large slag heaps have been identified. They have been carefully sampled, paying attention to the influence of weathering on the samples. The two heaps are located close to each other (at a distance of ca. 20 m.) and are mentioned in table 1 as M.La.1 and M.La.2. The amount of slag of both heaps has been estimated to weigh ca. 5 tons. The slag remains are scattered on an area of ca. 650 m^2.

The investigated samples from this area are samples which are optically dissimilar in their external appearance. The external surfaces are smooth and glassy, with noticeable flow structure on them. The flow structure suggests high viscosity and consequently high SiO_2-content in the liquid (Bachmann, 1982). The colour of the samples varies. Dominant colours observed are: black, dark red, green and -in many samples- bluish. The reddish slags could be identified as a reaction part between acidic slags and the furnace lining (Kronz & Eggers, 2001).

Residual charcoal from the burial remained in the texture of some pieces, and will be very helpful for dating the slags in future studies. Some of the slags show high porosity with respect to the high amount of volatile constituents, such as CO_2 and SO_3, during the cooling and slagging process. Typical samples from this area are shown in figure 4. Because of the lack of recent and systematic archaeological excavations in this region, no traces of furnaces and/or crucibles are reported in this region.

The analytical strategies used in this study are:

i. Quantitative X- ray diffraction for the identification of the crystalline phases with supplementary Rietveld refining methods.
ii. XRD for determining the bulk chemical composition.
iii. Optical microscopy in reflected as well as transmitted light for the mineralogical characterization as well as petrographic features.

Table 1.
Crystalline phase composition of the slags and their external properties

	Major Phases	Minor Phases	Trace Phases	color	Weight (g)	External Structure
M.Ls.1.01.06	Augite - Quartz - Amorphous	-	-	Black Blueish	138,9	Glassy with flow Structure, porous
M.Ls.1.02.06	Amorphous - Augite	Quartz - Cristobalite	-	Black	255,2	Glassy with flow Structure, porous
M.Ls.1.03.06	Amorphous - Augite	-	-	Black	524,6	Glassy with flow Structure, dense
M.Ls.1.04.06	Augite	Fayalite - Quartz - Cristobalite - Sanidine	-	Black	180,5	Glassy with flow Structure, dense
M.Ls.1.05.06	Fayalite	Augite - Magnetite	-	Black	729,5	Glassy with flow Structure, porous
M.Ls.1.06.06	Fayalite	Augite - Magnetite	-	Black	335	Glassy with flow Structure, porous
M.Ls.1.07.06	Amorphous - Cristobalite	Quartz - Augite	-	Black	74	Glassy with flow Structure
M.Ls.1.08.06	Augite - Amorphous - Cristobalite	-	Quartz	Dark Brown	50,8	Glassy with flow Structure, porous
M.Ls.1.09.06	Quartz - Schorl - Goethite	-	-	Dark Brown	224,6	Glassy with flow Structure, porous
M.Ls.1.10.06	Augite - Fayalite	-	-	Dark Brown	175,4	Glassy with flow Structure, porous
M.Ls.1.11.06	Wustite - Iron	Larnite - Magnetite	-	Dark Red	607,1	Glassy with flow Structure
M.Ls.1.12.06	Augite	Quartz - Sanidine	Brochantite	Dark Red	354,8	Glassy with flow Structure
M.Ls.1.13.06	Augite - Amorphous	Magnetite	Quartz	Dark Brown	720,7	Glassy with flow Structure,
M.Ls.1.14.06	Amorphous - Augite	-	-	Dark Brown	256,2	Glassy with flow Structure
M.Ls.1.15.06	Augite	-	Magnetite	Dark Brown	353,9	Compact structure dense
M.Ls.2.16.06	Augite	Magnetite	Quartz	Dark Brown	101,2	Compact structure and glassy
M.Ls.2.17.06	Augite - Quartz - Anorthite	-	Magnetite	Dark Brown	66,4	Compact structure and glassy
M.Ls.2.18.06	Amorphous	Cristobalite - Augite	Quartz	Dark Brown	101,2	Compact structure and glassy
M.Ls.2.19.06	Augite - Amorphous	Cristobalite	Quartz	Black	193,6	Compact structure and glassy
M.Ls.2.20.06	Augite	Magnetite - Brochantite	Quartz	Black Blueish	122,9	Compact structure and porous
M.Ls.2.21.06	Augite	Cristobalite	Quartz	Black Blueish	157,6	Compact structure and glassy
M.Ls.2.22.06	Augite - Fayalite	-	Quartz	Black Blue	493,1	Compact structure and glassy
M.Ls.2.23.06	Amorphous - Cristobalite - Augite	Quartz	-	Black	158,3	Compact structure and glassy
M.Ls.2.24.06	Augite	Amorphous	-	Dark Green	133,9	Compact structure with green malachite inclusions
M.Ls.2.25.06	Amorphous	Augite - Cristobalite	-	Black	509,3	Compact structure and glassy
M.Ls.2.26.06	Augite - Copper - Quartz	-	-	Dark Green	138,2	Compact structure with green malachite inclusions
M.Ls.2.27.06	Augite - Monticellite	Tenorite - Magnetite - Hematite	-	Dark Green	130,8	Compact structure with green malachite inclusions
M.Ls.2.28.06	Augite	Quartz	-	2.28.06	69,2	Compact structure, dense
M.Ls.2.29.06	Augite - Cristobalite	Quartz	-	Brown	358,5	Compact structure, dense
M.Ls.2.30.06	Amorphous - Augite - Cristobalite	-	-	Brown	611,5	Compact structure, dense

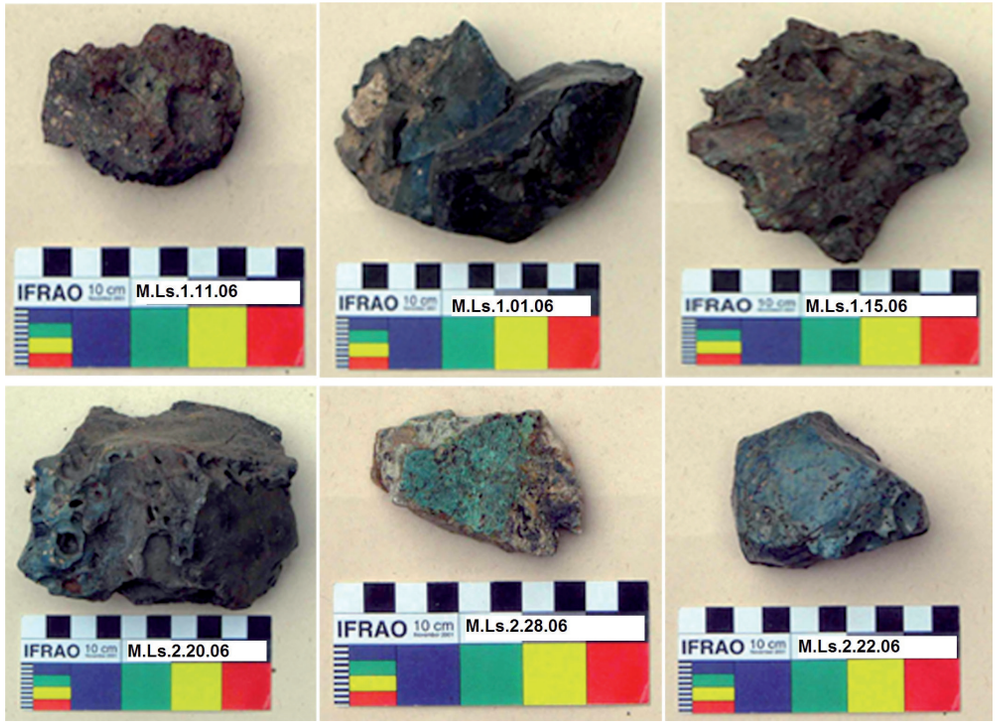

Figure 4. Sampled slags with their typical external features from Lasoleiman site.

iv. AFM for the investigation of the surface of glassy slags to identify the recrystallization or decomposition in the liquid. AFM is a method which is usually used for surface characterisation and hardness of inhomogeneous phase constituents. In addition, this method is used on these samples for characterising the crystalline phases in the melt.

RESULTS

3.1. X- ray fluorescence analysis

For the identification of bulk chemical composition of slags, 30 samples were analysed by the XRF method. The major oxides are SiO_2, FeO, CaO and Al_2O_3. To interpret the coexisting phases in the samples, the data were investigated in two main phase systems, namely CAfS and Cu-Fe-S; (C= $CaO+Na_2O+K_2O$, A= Al_2O_3, F = FeO+MnO+MgO + ZnO, S= SiO_2) (Keesmann, 1999; Hezarkhani & Keesmann, 1996).

In the CAFS system the oxides are measured in mol percent (Keesmann, Bachmann & Hauptmann, 1984). The chemical composition in Mol % is shown in Table 2. Based on this diagram the chemical compositions of major oxides in the samples are characterized as siliceous-calcium-iron rich slags (Figure 5). The point analyses proved that based on the CFS plane the material are rich in CaO, content and slightly Al_2O_3-poor. This composition has a tendency to form pyroxene and/or fayalite bearing slags. High amounts of CaO, and FeO, associated with SiO_2, can lead the composition toward the formation of some pyroxene phase closed to augite-hedenbergite composition (Hauptmann, 1985). Magnetite and wüstite have been detected in the samples, but because of the low amount of Al_2O_3, hercynite was not formed. Nevertheless, hercynite is not also detected by optical microscopy.

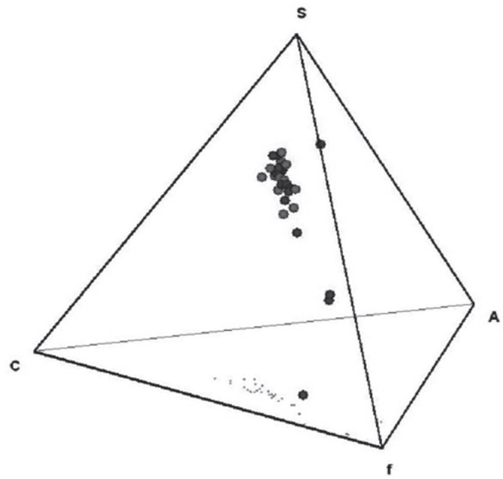

Figure 5. System SAfC and the composition of chemical composition of elements

Table 2.

Sample Number	SiO2	CaO	Al2O3	FeO+MnO+ MgO+ZnO
M.Ls.1.01.06	55,9	13,72	9,3	12,76
M.Ls.1.02.06	51,78	12,91	7,73	22,61
M.Ls.1.03.06	51,17	12,22	7,92	23,75
M.Ls.1.04.06	47,1	13,8	7,86	24,94
M.Ls.1.05.06	26,93	5,74	1,93	55,86
M.Ls.1.06.06	28,27	5,25	1,73	55,14
M.Ls.1.07.06	59,75	15,19	7,19	14,37
M.Ls.1.08.06	54,24	14,71	7,28	18,19
M.Ls.1.09.06	64,57	1,18	6,48	23,59
M.Ls.1.10.06	40,73	11,59	4,92	36,04
M.Ls.1.11.06	5,87	15,79	1,48	67,47
M.Ls.1.12.06	51,83	13,25	9,33	16,39
M.Ls.1.13.06	55,07	13,31	6,26	18,14
M.Ls.1.14.06	51,6	14,33	8,3	20,96
M.Ls.1.15.06	50,41	12,39	6,73	25
M.Ls.2.01.06	52,66	18,96	8,72	14,72
M.Ls.2.02.06	55	13,56	10,55	14,05
M.Ls.2.03.06	56,17	14,1	6,85	18,48
M.Ls.2.04.06	53,2	14,45	8,11	19,28
M.Ls.2.05.06	48,93	10,09	6,61	25,04
M.Ls.2.06.06	51,26	13,28	8,61	22,27
M.Ls.2.07.06	46,58	11,88	7,28	28,96
M.Ls.2.08.06	60,17	12,03	6,04	16,47
M.Ls.2.09.06	43,22	15,3	9,62	25,42
M.Ls.2.10.06	55,34	16,94	8,74	14,61
M.Ls.2.11.06	47,6	15,62	10,85	18,14
M.Ls.2.12.06	51,85	13,27	8,87	20,55
M.Ls.2.13.06	53,48	15,56	7,97	17,84
M.Ls.2.14.06	54,57	11,64	6,85	18,26
M.Ls.2.15.06	56	13,17	8,32	17,37

One of the important systems for determining the sulphidic fraction of slags is the Cu-Fe-S system (Figure 6 and Table 3). This system often summarizes the composition of sulphidic ores and the quality of smelting process for removing sulphide impurities from the extracted ore (Bachmann, 1982). According to this diagram some points could be highlighted as follows:

1. The samples are Fe-rich and the Cu is a coexisting phase derived from chalcopyrite ore relics (Emami, 2005).

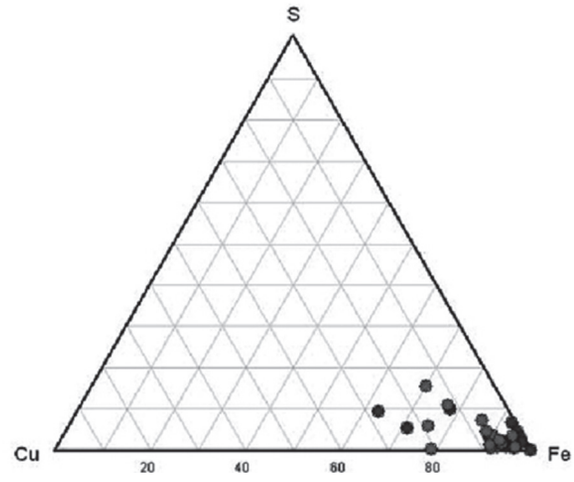

Figure 6. System Cu-Fe-S for determining the distribution of sulphides in the slags

Table 3.

Bulk chemical analysis of slags in system Cu-Fe-S in W %.

	S	Fe	Cu
M.Ls.1.01.06	0,55	8,518	4,076
M.Ls.1.02.06	0,162	16,119	0,792
M.Ls.1.03.06	0,061	16,966	0,711
M.Ls.1.04.06	0,272	18,415	1,639
M.Ls.1.05.06	1,345	42,968	0,436
M.Ls.1.06.06	0,882	42,345	0,361
M.Ls.1.07.06	0,075	9,68	0,56
M.Ls.1.08.06	0,168	12,885	1,157
M.Ls.1.09.06	0,224	17,008	0,133
M.Ls.1.10.06	0,228	27,157	0,355
M.Ls.1.11.06	0,004	52,277	0,013
M.Ls.1.12.06	0,384	11,549	4,168
M.Ls.1.13.06	0,729	13,011	2,209
M.Ls.1.14.06	0,165	15,335	0,478
M.Ls.1.15.06	0,055	18,212	1,064
M.Ls.2.01.06	0,371	10,233	0,906
M.Ls.2.02.06	0,338	9,834	2,718
M.Ls.2.03.06	0,03	13,018	0,483
M.Ls.2.04.06	0,256	13,76	1,061
M.Ls.2.05.06	1,164	18,422	3,166
M.Ls.2.06.06	0,254	16,119	0,389
M.Ls.2.07.06	0,059	21,242	0,727
M.Ls.2.08.06	0,272	11,927	1,058
M.Ls.2.09.06	0,068	18,226	1,462
M.Ls.2.10.06	0,018	9,897	0,978
M.Ls.2.11.06	0,005	12,542	3,687
M.Ls.2.12.06	0,094	15,209	1,519
M.Ls.2.13.06	0,084	12,738	0,831
M.Ls.2.14.06	1,292	13,312	3,062
M.Ls.2.15.06	0,141	12,305	0,783

2. With respect to the low amounts of Cu and S in most of the samples, no high amounts of copper sulphide phases in the samples are present. This is due to the extraction of Cu under roasting-reducing process (Blanderer, 1964; Marechal, 1985).

According to figure 3, the reaction has been done in two steps according to the sulfidic ores (Rehren *et al*., 2012).

I. Roasting the ore (partial smelting)

- *Cu2S + 2O2 → CuO + SO2*
- *2FeS + 3O2 → 2FeO + 2SO2*

II. Smelting for matte and slag forming

a) CO does not reduce Cu_2S or FeS. It forms matte or (Copper-stone) which consists of different sulphides such as: Cu_2S, CuS, Fe_2S, FeS.

b) *2FeO + SiO2 → 2FeO.SiO2 (Slag)*

c) *CuO + CO → Cu (Metal) + CO2 ↑*

The entire results of the bulk chemical composition of major, minor and trace elements are given in the Table 4. Surprisingly, the amount of As, in the slags is very low.

Qualitative and quantitative X- ray diffraction analysis

To elucidate the exact crystalline structure of the phases, XRD analysis was performed qualitatively using an instrument from PANalytical X'Pert Pro Power. 10 samples have been analysed with XRD and refined with Rietveld refining methods to determine the best preferred orientation of constituent's minerals with respect to the factor of degree of fitness of each phase. Figure 7a, shows the general results of the XRD analysis with the major crystalline phases in the matrix of slags.

The results of quantitative phase refinements and the ICSD number of all phases are given in Table 5. The crystalline phases are classified in three groups; as the phases which existed before melting, the phases which occurred during the melting and smelting, as well as the phases which occurred after the metallurgical process. The last group are those that mainly consist of oxides or weathering products. The results prove that pyroxene as Augite ($Ca(Fe,Mg)Si_2O_6$), Clinoferrosilite ($FeSiO_3$), fayalite (Fe_2SiO_4) and cristobalite (SiO_2) are the dominant phases in the samples. Tridymite is not expected by increasing the temperature and decomposed rapidly to cristobalite due to amount of impurity in the raw material. Larnite and monticellite from the olivine group also contain mainly iron-bearing phases within the slags.

Furthermore, magnetite (Fe_3O_4) and cristobalite (SiO_2) are remarkable phases that occurred via rapid smelting. Wüstite and hematite formed in the matrix during the cooling process in oxidising conditions. These phases oc-

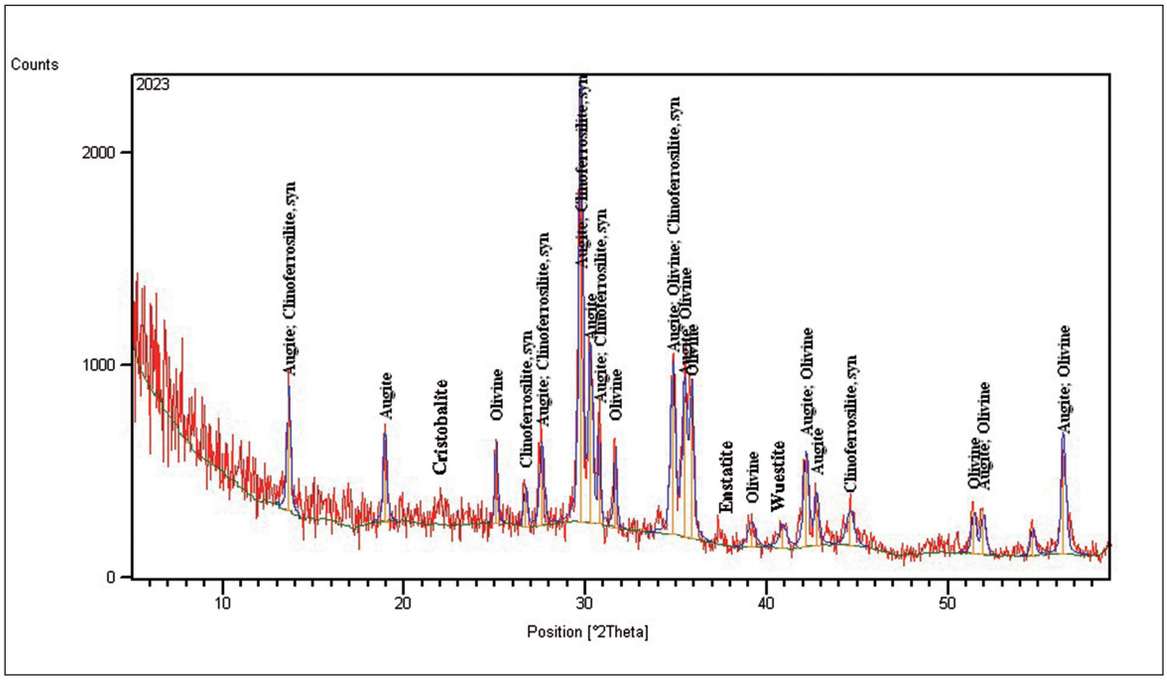

Figure 7a. Diffractogram of one sample with all calculated phases in their best preferred orientation.

Table 4.

Balk chemical analysis of major, minor and trace elements of the slags from two Lasoleiman heaps in weight percent

	CuO	ZnO	Cl	S	Ba	Sr	Pb	V	Ce	W	Nb	Zr	Y	Rb	Ni	Cr
	W%	W%	W%	W%	W%	W%	W%	W%	W%	W%	W%	W%	W%	W%	W%	W%
M.Ls.1.01.06	5.099	0.257	0.0148	0.5499	0.0801	0.0441	0.0535	0.0067	0.0061	0.0001	0.0010	0.0106	0.0007	0.0056	0.0035	0.0045
M.Ls.1.02.06	0.991	0.616	0.0019	0.1620	0.0740	0.0225	0.0463	0.0065	0.0021	0.0001	0.0004	0.0065	0.0007	0.0060	0.0028	0.0030
M.Ls.1.03.06	0.890	0.087	0.0005	0.0607	0.0421	0.0345	0.0174	0.0077	0.0024	0.0001	0.0006	0.0076	0.0002	0.0052	0.0030	0.0045
M.Ls.1.04.06	2.050	0.051	0.0028	0.2722	0.0400	0.0325	0.0065	0.0069	0.0032	0.0001	0.0003	0.0061	0.0001	0.0048	0.0028	0.0032
M.Ls.1.05.06	0.546	0.344	0.0006	1.3446	0.4102	0.0157	0.0002	0.0088	0.0035	0.0001	0.0001	0.0032	0.0002	0.0023	0.0024	0.0025
M.Ls.1.06.06	0.451	0.427	0.0036	0.8819	0.4022	0.0141	0.0004	0.0083	0.0030	0.0001	0.0008	0.0039	0.0001	0.0021	0.0026	0.0026
M.Ls.1.07.06	0.700	0.600	0.0016	0.0752	0.0733	0.0507	0.0077	0.0059	0.0047	0.0001	0.0002	0.0085	0.0005	0.0066	0.0030	0.0028
M.Ls.1.08.06	1.448	0.209	0.0058	0.1675	0.0888	0.0336	0.0248	0.0064	0.0021	0.0001	0.0002	0.0068	0.0005	0.0058	0.0033	0.0030
M.Ls.1.09.06	0.167	0.005	0.0215	0.2236	0.0154	0.0091	0.0071	0.0109	0.0012	0.0001	0.0004	0.0103	0.0004	0.0017	0.0031	0.0027
M.Ls.1.10.06	0.444	0.263	0.0007	0.2284	0.2385	0.0228	0.0045	0.0075	0.0037	0.0001	0.0012	0.0056	0.0002	0.0040	0.0024	0.0030
M.Ls.1.11.06	0.016	0.002	0.0268	0.0040	0.0230	0.0204	0.0008	0.0029	0.0030	0.0001	0.0005	0.0029	0.0002	0.0019	0.0033	0.0017
M.Ls.1.12.06	5.214	0.229	0.0073	0.3840	0.0749	0.0390	0.0459	0.0061	0.0068	0.0001	0.0002	0.0091	0.0005	0.0055	0.0030	0.0045
M.Ls.1.13.06	2.763	0.237	0.0038	0.7287	0.0922	0.0288	0.0287	0.0065	0.0078	0.0001	0.0008	0.0072	0.0006	0.0055	0.0030	0.0030
M.Ls.1.14.06	0.598	0.024	0.0051	0.1652	0.1078	0.0515	0.0036	0.0089	0.0043	0.0001	0.0002	0.0097	0.0008	0.0058	0.0025	0.0038
M.Ls.1.15.06	1.331	0.172	0.0014	0.0552	0.0483	0.0266	0.0381	0.0062	0.0035	0.0001	0.0007	0.0066	0.0004	0.0051	0.0029	0.0028
M.Ls.2.01.06	1.133	0.115	0.0152	0.3709	0.1048	0.0356	0.0067	0.0061	0.0050	0.0390	0.0005	0.0083	0.0007	0.0050	0.0024	0.0027
M.Ls.2.02.06	3.400	0.040	0.0049	0.3375	0.0700	0.0388	0.0155	0.0071	0.0041	0.0001	0.0008	0.0106	0.0009	0.0055	0.0034	0.0057
M.Ls.2.03.06	0.604	0.367	0.0005	0.0301	0.0939	0.0333	0.0311	0.0061	0.0025	0.0001	0.0013	0.0089	0.0007	0.0061	0.0033	0.0028
M.Ls.2.04.06	1.327	0.066	0.0096	0.2564	0.0746	0.0398	0.0066	0.0075	0.0022	0.0001	0.0004	0.0092	0.0004	0.0061	0.0032	0.0042
M.Ls.2.05.06	3.961	0.129	0.0044	1.1641	0.0378	0.0235	0.0303	0.0063	0.0056	0.0001	0.0003	0.0050	0.0003	0.0052	0.0029	0.0024
M.Ls.2.06.06	0.487	0.034	0.0013	0.2541	0.0670	0.0373	0.0036	0.0083	0.0015	0.0001	0.0007	0.0085	0.0003	0.0066	0.0031	0.0042
M.Ls.2.07.06	0.909	0.043	0.0052	0.0594	0.0385	0.0271	0.0118	0.0092	0.0025	0.0001	0.0003	0.0067	0.0006	0.0043	0.0035	0.0079
M.Ls.2.08.06	1.324	0.038	0.0052	0.2715	0.0739	0.0277	0.0044	0.0058	0.0019	0.0001	0.0013	0.0074	0.0005	0.0064	0.0028	0.0020
M.Ls.2.09.06	1.829	0.033	0.0037	0.0675	0.0494	0.0325	0.0076	0.0071	0.0025	0.0001	0.0007	0.0087	0.0006	0.0043	0.0038	0.0066
M.Ls.2.10.06	1.224	0.072	0.0018	0.0176	0.0652	0.0435	0.0228	0.0079	0.0037	0.0001	0.0002	0.0093	0.0008	0.0064	0.0025	0.0045
M.Ls.2.11.06	4.613	0.041	0.0002	0.0045	0.0545	0.0414	0.0144	0.0071	0.0030	0.0001	0.0014	0.0101	0.0007	0.0045	0.0036	0.0072
M.Ls.2.12.06	1.900	0.030	0.0052	0.0937	0.0656	0.0481	0.0084	0.0058	0.0027	0.0001	0.0008	0.0083	0.0002	0.0042	0.0032	0.0029
M.Ls.2.13.06	1.040	0.094	0.0032	0.0840	0.0702	0.0435	0.0095	0.0064	0.0035	0.0001	0.0002	0.0087	0.0003	0.0063	0.0033	0.0036
M.Ls.2.14.06	3.830	0.030	0.0056	1.2921	0.0665	0.0259	0.0047	0.0061	0.0069	0.0001	0.0001	0.0067	0.0001	0.0061	0.0029	0.0034
M.Ls.2.15.06	0.979	0.053	0.0017	0.1410	0.0828	0.0432	0.0105	0.0090	0.0042	0.0001	0.0002	0.0104	0.0005	0.0064	0.0033	0.0046

Table 4. (Continuation)

Balk chemical analysis of major, minor and trace elements of the slags from two Lasoleiman heaps in weight percent

	Co	As	U	Th	SiO_2	Al_2O_3	FeO	CaO	Na_2O	K_2O	MgO	TiO_2	MnO	P_2O_5	Total
	W%	W%	W%	W%	W%	W%	W%	W%	W%	W%	W%	W%	W%	W%	**W%**
M.Ls.1.01.06	0.0017	0.0035	0.0006	0.0017	55.900	9.300	10.954	10.880	0.390	2.450	1.490	0.246	0.063	0.094	97.912
M.Ls.1.02.06	0.0019	0.0039	0.0006	0.0018	51.780	7.730	20.729	9.900	0.580	2.430	1.170	0.207	0.097	0.106	96.679
M.Ls.1.03.06	0.0038	0.0022	0.0004	0.0007	51.170	7.920	21.818	9.550	0.520	2.150	1.730	0.276	0.119	0.080	96.504
M.Ls.1.04.06	0.0025	0.0012	0.0005	0.0008	47.100	7.860	23.681	11.770	0.010	2.020	1.120	0.191	0.089	0.097	96.426
M.Ls.1.05.06	0.0048	0.0015	0.0007	0.0015	26.930	1.930	55.257	4.810	0.210	0.720	0.250	0.085	0.013	0.040	92.937
M.Ls.1.06.06	0.0052	0.0012	0.0006	0.0013	28.270	1.730	54.455	4.340	0.250	0.660	0.240	0.077	0.014	0.034	92.282
M.Ls.1.07.06	0.0015	0.0009	0.0006	0.0007	59.750	7.190	12.448	12.080	0.700	2.410	1.250	0.172	0.071	0.070	97.686
M.Ls.1.08.06	0.0019	0.0023	0.0006	0.0011	54.240	7.280	16.571	11.990	0.450	2.270	1.330	0.177	0.078	0.097	96.494
M.Ls.1.09.06	0.0060	0.0029	0.0003	0.0011	64.570	6.480	21.872	0.560	0.370	0.250	1.710	0.358	0.006	0.100	96.766
M.Ls.1.10.06	0.0039	0.0026	0.0006	0.0012	40.730	4.920	34.924	9.120	0.450	2.020	0.790	0.174	0.060	0.079	94.504
M.Ls.1.11.06	0.0012	0.0019	0.0007	0.0016	5.870	1.480	67.228	15.470	0.130	0.190	0.240	0.052	0.003	0.088	90.866
M.Ls.1.12.06	0.0028	0.0024	0.0005	0.0017	51.830	9.330	14.852	9.920	0.010	3.320	1.250	0.244	0.064	0.124	96.981
M.Ls.1.13.06	0.0016	0.0024	0.0007	0.0013	55.070	6.260	16.733	11.320	0.010	1.980	1.100	0.161	0.074	0.093	96.723
M.Ls.1.14.06	0.0027	0.0041	0.0009	0.0011	51.600	8.300	19.721	11.290	0.690	2.350	1.150	0.196	0.065	0.085	96.447
M.Ls.1.15.06	0.0025	0.0026	0.0004	0.0016	50.410	6.730	23.420	10.190	0.300	1.900	1.280	0.159	0.132	0.070	96.299
M.Ls.2.01.06	0.0015	0.0034	0.0023	0.0023	52.660	8.720	13.159	16.720	0.360	1.880	1.330	0.175	0.111	0.138	97.114
M.Ls.2.02.06	0.0016	0.0098	0.0006	0.0014	55.000	10.550	12.646	10.560	0.750	2.250	1.290	0.290	0.070	0.109	97.474
M.Ls.2.03.06	0.0010	0.0039	0.0005	0.0010	56.170	6.850	16.742	11.360	0.590	2.150	1.290	0.172	0.086	0.105	96.713
M.Ls.2.04.06	0.0024	0.0044	0.0004	0.0006	53.200	8.110	17.696	11.030	0.610	2.810	1.440	0.211	0.075	0.103	97.106
M.Ls.2.05.06	0.0034	0.0038	0.0007	0.0016	48.930	6.610	23.690	8.170	0.010	1.910	1.100	0.160	0.123	0.069	96.160
M.Ls.2.06.06	0.0023	0.0035	0.0008	0.0013	51.260	8.610	20.729	9.660	0.620	3.000	1.390	0.275	0.115	0.117	96.702
M.Ls.2.07.06	0.0032	0.0025	0.0007	0.0015	46.580	7.280	27.318	9.580	0.390	1.910	1.440	0.254	0.161	0.125	96.175
M.Ls.2.08.06	0.0024	0.0010	0.0005	0.0009	60.170	6.040	15.338	9.060	0.390	2.850	1.030	0.164	0.062	0.106	96.987
M.Ls.2.09.06	0.0050	0.0017	0.0006	0.0015	43.220	9.620	23.438	12.220	0.840	2.240	1.880	0.275	0.069	0.135	96.003
M.Ls.2.10.06	0.0022	0.0030	0.0003	0.0009	55.340	8.740	12.727	12.980	0.980	2.980	1.730	0.222	0.083	0.094	97.365
M.Ls.2.11.06	0.0044	0.0006	0.0007	0.0013	47.600	10.850	16.130	12.340	1.080	2.200	1.910	0.293	0.059	0.133	97.408
M.Ls.2.12.06	0.0045	0.0015	0.0005	0.0010	51.850	8.870	19.559	10.920	0.280	2.070	0.910	0.177	0.049	0.105	96.977
M.Ls.2.13.06	0.0020	0.0023	0.0005	0.0009	53.480	7.970	16.382	12.420	0.560	2.580	1.290	0.198	0.077	0.102	96.441
M.Ls.2.14.06	0.0032	0.0026	0.0004	0.0009	54.570	6.850	17.120	8.640	0.010	2.990	1.060	0.206	0.050	0.110	96.900
M.Ls.2.15.06	0.0023	0.0021	0.0006	0.0015	56.000	8.320	15.824	10.350	0.610	2.210	1.400	0.288	0.089	0.105	96.552

Table 5.
Quantitative measurments of crystaline phases after Rietveld refining method in W%.
The best matched crystal structure is given after ICSD

	ICSD No.	W%	Best Prefered Orientation	hkl
Cristobalite	44094	0.3-16	2Θ = 22.049	101
Augite	55921	7.2-42	2Θ = 29.795	22-1
Diopside	64977	33-67.7	2Θ = 27.451	221
Clinoferrosilite	20391	0.4-9.8	2Θ = 29.352	021
Enstatite	24464	5.2-24.9	2Θ = 38.135	042
Olivine	66191	0.9-4.7	2Θ = 31.598	121
Wuestite	76639	0.8-2.1	2Θ = 41.867	200

cur in the matrix and do not have a well preferred orientation via fitting for calculation of their crystal structure. Goethite, metallic copper and iron are also seen in the microscopic picture but they were not measured in powder samples. The identified phases in these samples are common minerals found in magmatic rocks and are seen in granites, granodiorites and other magmatic stones (Klein & Hurlbut Jr., 1999). The isoline diagram of all samples shows their variation of phase constituents around 2Θ ~ 28-35° in the figure 7b.

Phase determination and interpretation of paragenesis by Microscopic

Investigations

Petrographic studies give more results on the investigated samples, due to the different composition of crystals as well as different metallic relics in the texture. The results are presented on the basis of identified phases.

- **Silicates**

Pyroxenes and olivine are observed in almost all samples. The distribution of these phases in samples may suggest a homogenous smelting process and a high amount of silicate phases. The variations in colour of the pyroxene in samples are caused by concentrations of Ca, Mg and Fe ions within the crystal structure of pyroxene (Figure 8). Different modifications of pyroxenes, such as augite, hedenbergite, diopside or wollastonite, are observed in the samples. Pyroxene observed in these samples has a "horse tail" structure, and is commonly associated with the copper smelting technology in central Iran (Emami, 2006). Olivine is observed as fayalite in prismatic or plate habitus (Figure 9). Fayalite formed mostly as idiomorphic structure. The formation temperature of fayalite is

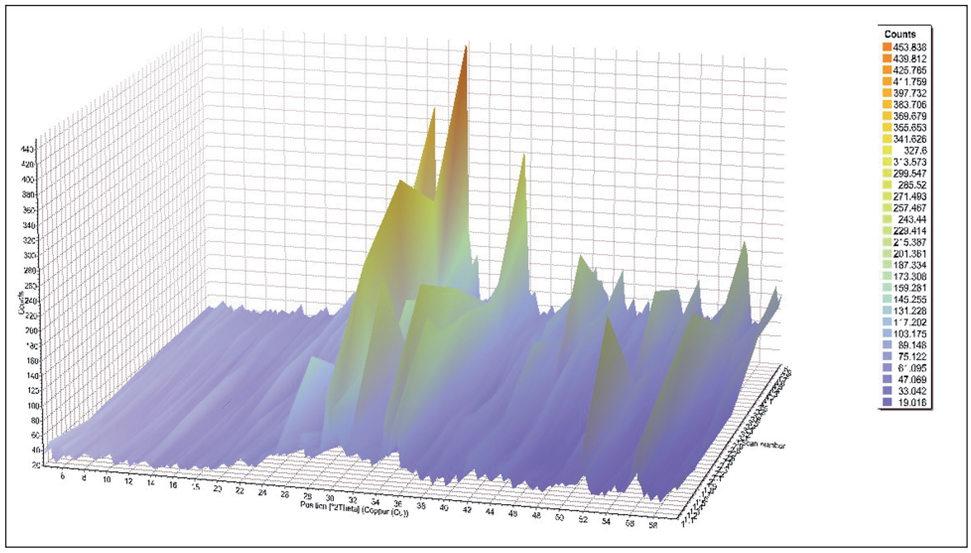

Figure 7b. Diffractogram of one sample with all calculated phases in their best preferred orientation.

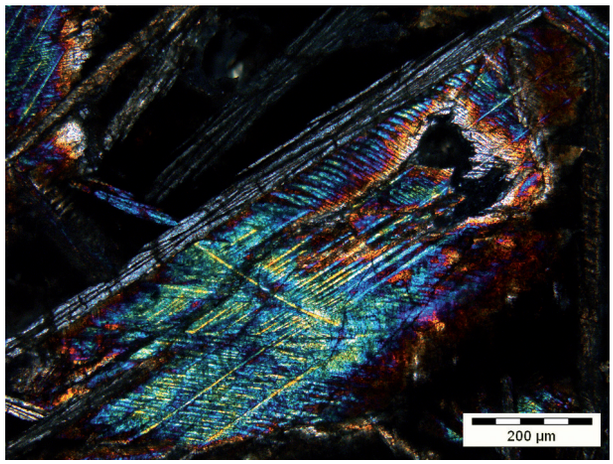

Figure 8. Sample No. M.Ls.1.05.06. Pyroxene crystals with high amount of Fe (augite) that show by succession of colours x 10,2 pol.

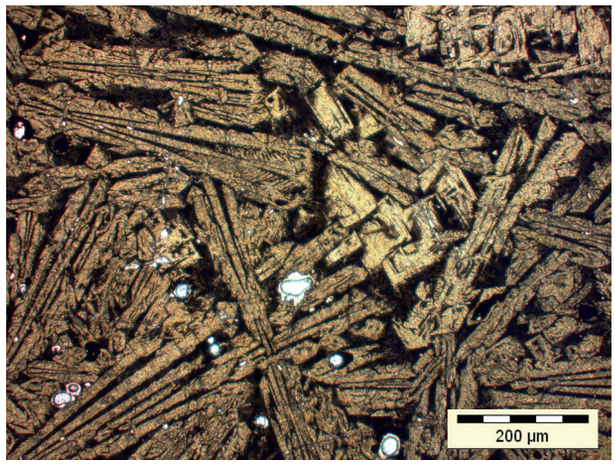

Figure 9. Sample No. M.Ls.2.11.06. Fayalite crystals in dendritic form. In these crystals the Fe % is low and this is occurred in many of the slag samples. No. 2. ×10, 2 pol

about 950°C. Magnetite crystallized on top of the fayalite due to the existence of Fe delivered from the fayalite during the oxidation process. The bipyramidal structure of fayalite is a reason for the high viscosity of the melt (Moorey, 1988).

- ***Oxides and Sulphides***

The common oxides in the samples suggest that there are iron oxides in different ionic charges. This may have occurred because of the high percentage of iron in the slag composition. Magnetite, hematite and limonite are also detected in the matrix as accumulations of these phases in and around the pores. Magnetite appears around the fayalite - and not above it - due to the oxidation of fayalite. Iron oxide formed as wüstite (FeO), because of reducing conditions and low oxygen fugacity (low fO_2) (Figure 10). Wüstite is stable under 570°C (Kronz & Eggers, 1991; Klein et al., 1999).

Sulphides remain mostly unchanged in slags and can be used for identifying the ores originally used and the probable method applied for the extraction of metal from these ores. Chalcocite is a very common ore in ancient copper extraction in Iran (Emami 2006). Chalcopyrite-digenite-bornite is the typical structure detected in the samples (Figure 11). Bornite as an anisotropic pink phase, digenite as a blue isotropic phase and chalcopyrite as a yellow aggregate are observed. Chalcopyrite in this circumstance is detected as secondary chalcopyrite that appeared around the external boundaries of bornite (pink in figure 11).

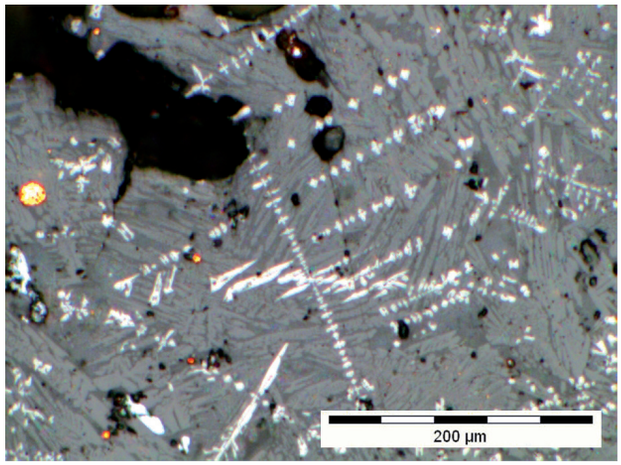

Figure 10. A micrograph of polished section of Sample M.Ls.2.09.06. Dendritic wüstite forms on pyroxene crystals in reducing conditions. ×20, 1 pol.

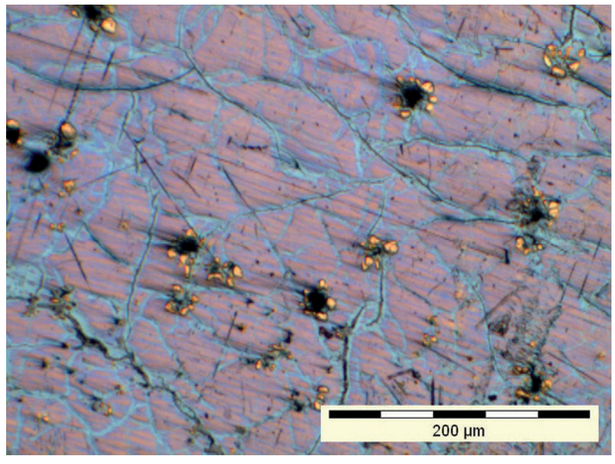

Figure 11. Sample M.Ls.1.11.06. Chalcopyrohtine (light yellow), chalcocite (blue-grey) and bornite (pink partially), the eutectic phase is visible in the center of image. ×20, 2 pol.

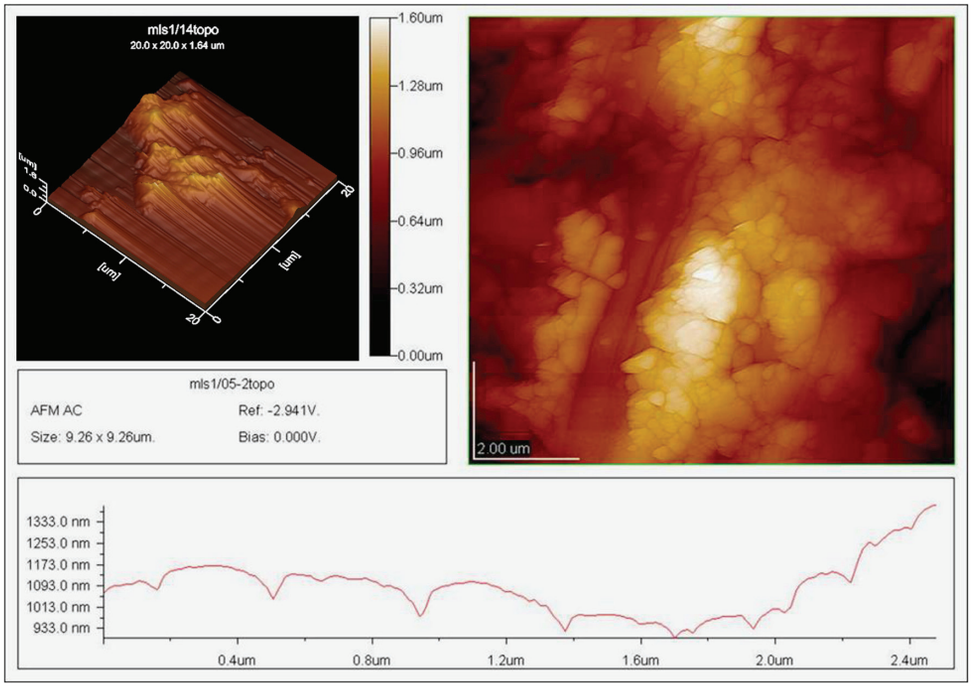

Figure 12. AFM scan area in AC mode for detection of magnetite crystals on the fayalite grain in the glassy matrix.

The stability areas of these phases are between 850-930°C, but - depending on Cu-As composition of the eutecticum,– they can change and reach a temperature of approximately 690°C (Keesmann & Moreno Onorato, 1999). Chalcopyrite is well defined in the samples. The presence of chalcocite and chalcopyrohtine associated with bornite is well-known in the eutecticum of the system Fe-Cu-S.

In order to interpret the morphologic deformation of nanoscopic areas, atomic force microscopy methods were applied. The investigations were carried out in non-contact mode. Measurements and additional physical properties (viscosity, rigidity, adhesion, etc.) can be obtained from the phase decomposition based on cantilever oscillations (Emami et al., 2007). This allows the quantification of the physical and chemical homogeneity of the material's surface. With this data, it is possible to examine the dissolution and phase transition in the iron-rich matrix based on challenges in the face-interface area (Figure 12). The roughness of the surface at the nano-scale is measured based on the defects caused through the expansion process. Here, a nanoscopic polycrystalline matrix on the external surface of fayalite and the formation of magnetite as an oxidation product are observed. As mentioned before, with these methods it is possible to detect the tiny crystals of magnetite that formed around the fayalite and not above it.

CONCLUSION

The analyses presented in this paper are preliminary results based on archaeo-metallurgical data, and give an overview of the metallurgical processes executed in the Meymand region. The high percentage of SiO_2 in samples, which is associated with other oxides such as Al_2O_3, FeO, CaO and MgO, suggest that they are probably remains of ores smelted on this site.

The metallurgical process in Meymand can be related to copper smelting of copper-iron sulphide polymetallic ores. The ores contain a high amount of sulphides and a considerable percentage of Fe. As a matter of fact the extractive metallurgy of sulphide ores was known after oxides were experimented with by human by the end of the first millennium BC. Accordingly, the metallurgical process is well known in this area and will not be older that 1st millennium BC. The extraction was carried out via roasting and matte forming to the reduction of copper sulphide. Indeed the extraction of copper seems to review very well due to the high amount of iron in the rest smelted materials.

The extractive metallurgy carried out on both slag deposits was similar with respect to the paragenesis of different copper sulphides in different stages, which present digenite-chalcopyrite as well as digenite-bornite-cha-

lkopyrite paragenesis. This is an equilibrium system in solid solution and consists of slag, ore and deposited phases. The main technology in this area was roast-reduction of copper, due to the forming of copper sulphides around metallic copper and pyrite or magnetite. This process was followed by roasting and matte formation. The temperature was between 750 to 950°C based on the stability region of the phases. The granite and granodiorite rocks of this area were the main economic bearing metals used for the extractive process.

ACKNOWLEDGEMENTS

The Authors would like to thank Kiarash Eqtesadi, the manager, and Mehrdad Mehran, Amin Keyvanloo, Hossein Mahmoodi and Hassan Ebrahimi, staffs of Meymand Cultural Heritage and Tourism Base, ICHTO, for their helps in different stages of this research.

This research was funded by Meymand Cultural Heritage and Tourism Base, ICHTO. The chemical experiments were executed in Kansaran-e Binaloud Co. Tehran.

REFERENCES

Bachmann, H. G. (1982): "*The identification of slags from archaeological site"*, Occasional Publications No.6, Institute of Archaeology, London.

Blanderer, K. (1964): "*Apparatus for removal of impurity components from sulphidic and metallized molten copper mattes*", Erzmetall, XVII, p.247-253.

Ebrahimi Meymand, H. (2002): "*Research report about Meymand Geographical locations*", Meymand Cultural Heritage and Tourism Base. (In Farsi)

Emami, M. (2005): "*Experimental and petrological studies of ancient slags to define the paragenesis of ore deposits*", Year Book of Iranian Mining Engineer, vol. 1, p.63-78.

Emami, M. (2006): "*Phase transition induced by solid solution in the pyroxene-rich ancient copper slags from Toroud, Iran*", Proceeding for International Symposium of Archaeometallurgy, Canada.

Emami, M., Volkmar, J. and Trettin, R. (2007): "*Quantitative characterization of damage mechanisms in ancient ceramics by quantitative x-ray powder diffraction (QXRD), polarization microscopy, confocal laser scanning microscopy (CLSM) and non-contact mode atomic force microscopy (AFM)*", Surface Modification Technologies XXI, Edited by T. S. Sudarshan and M. Jeandin, © ASM International, Materials Park, Ohio, USA.

Hauptmann, A. (1985): "*Die Entwicklung der Kupfermetallurgie vom 3. Jahrtausend bis zur Neuzeit. 5000 Jahre Kupfer im Oman*", Der Anschnitt, Beiheft 4, Bochum.

Hezarkhani, Z. Keesmann, I. (1996): "*Archäometallurgische untersuchungen im gebiet von Saghand-Posht-e-Badam (Zentraliran)*", Metalla (Forschungsberichte des Deutschen Bergbau-Museums, Bochum), (1996/3.2), 101-125.

Izadpanah, F. (2002): "*Architecture studies in Meymand historical village*", ICHO. (In Farsi)

Keesmann, I., Moreno Onorato, A. (1984): "*Naturwissenschaftliche Untersuchungen zur früher Technologie von Kupfer und Kupfer-Arsen-Bronze*", Der Anschnitt, Beiheft 9, S. 317-333.

Keesmann, I. (1999): "*Schlacken verschiedener stufen der Eisentechnologie. Prehistoric and Medieval Direct Iron Smelting in Scandinavia and Europe*", CPSA - Jutland Conference Sandbjerg, September 16-20.

Keesmann, I., Bachmann, H., & Hauptman, A. (1984): "*Klassifikation eisenreicher Schlacken nach dem, Fortschritt der Mineralogie*", 62 Beiheft 1, p.114-116.

Kronz, A. & Eggers, T. (2001): "*Archäologische Untersuchungen eisenzeitlicher Funde aus dem Hügelgräberfeld Hillesheim, Kreis Daun*", Trierer Zeitschrift 64. Trier

Klein, C., Hurlbut Jr., C. S. (1999): "*Manual of mineralogy*", (After James D. Dana), John Wiley & Sons, Inc. 21st Edition, Revised.

Marechal, J.R. (1985): "*Methods of Ore Roasting and the Furnace Used (Trans. by P.T. Craddock)*". In P.T. Craddock and M.J. Hughes (eds.), Furnace and Smelting Technology in Antiquity. British Museum Occ. Paper 48.29-42

Moorey, P.R.S. (1982): "*The archaeological evidence for metallurgy and relate technologies in Mesopotamia c. 5500-2100 BC*", Iraq 44, p.13-38.

Ness, W. D. (2004): "*Introduction to Optical Mineralogy*", Third Edition, Oxford University Press.

NGO of I.R.IRAN. (2003): "*National gazetteer of the I.R of Iran Kerman province*", Shahrebabak Township, 10th vol. National Geographical Organization of I.R.IRAN Publications, Tehran. (In Farsi).

Rehren, T., Boscher, L., and Pernicka, L. (2012): "*Large scale smelting of speiss and arsenical copper at Early Bronze Age Arisman, Iran*", Journal of Archaeological Science, vol. 39,pp. 1717-1727.